INTERNATIONAL JOURNAL OF AUTOMOTIVE AND MECHANICAL ENGINEERING (IJAME)
ISSN: 2229-8649 e-ISSN: 2180-1606
VOL. 17, ISSUE 2, 7842 – 7850
DOI: https://doi.org/10.15282/ijame.17.2.2020.03.0584

ORIGINAL ARTICLE

Thermal Profile and Microstructure of Wrought Aluminium 7075 for Semisolid Metal Processing

N. A. Razak[1*], A. H. Ahmad[1] and M. M. Rashidi[2]

[1]Department of Mechanical Engineering, College of Engineering, Universiti Malaysia Pahang, Lebuhraya Tun Razak, 26300 Gambang, Kuantan, Pahang, Malaysia
Phone: +6094246273; Fax: +6095492689
[2]Faculty of Mechanical and Automotive Engineering Technology, Universiti Malaysia Pahang, 26600 Pekan, Pahang, Malaysia

ABSTRACT – Thermal analysis (TA) is a non-damaging and quick method to check the molten metal's condition preceding to casting. This paper aims to present the relationship between fraction solid and temperature by utilising cooling curve analysis (CCA), to acquire correct processing parameters for wrought aluminium 7075 in semisolid condition. An induction furnace was used to heat a graphite crucible containing wrought aluminium 7075 alloy up to the temperature of 750 °C. A calibrated Chromel-Alumel K-type thermocouple was placed at the centre of the crucible and was submerged to 15 mm in the melt. The solidification temperature and time were measured by Data Logger GL-220. Normal, intermediate, and high cooling rate conditions were achieved when the crucible was left in an open atmosphere, in an open atmosphere with additional minimum airflow, and in an open atmosphere with the maximum airflow, respectively. It was found that the normal cooling rate was estimated at 2.23 °C/s, the intermediate cooling rate was calculated at 2.88 °C/s while the high cooling rate was recorded at 3.20 °C/s. The increase in cooling rate conditions has a significant effect on the changes of phases during solidification process where it leads to the decreased in liquidus, eutectic and solidus temperature. The microstructure feature was found to have a significant difference with the variation of cooling rates where higher cooling rate led to smaller primary grain size.

ARTICLE HISTORY
Revised: 7th April 2020
Accepted: 5th May 2020

KEYWORDS
Sem-solid metal;
Thermal analysis;
Cooling rate;
Aluminium 7075;
Globular microstructure.

INTRODUCTION

Increasing demands for improving structural efficiency, from both automotive and aeronautic/aerospace industry, has focused designers' attention on enhancing material performance through the development of lighter weight, stiffer, and/or stronger material [1]. Aluminium alloys are considered as one of the potential candidates for the demand for lightweight alloys in those applications. Most of the automotive components in automotive power trains (intake manifolds, transmission housings, engine blocks, cylinder heads and pistons) and chassis application (wheels, brackets, brake components, and instrument panels) are made from aluminium alloys, which utilised conventional metal casting processes [2, 3]. However, the conventional casting process has its shortcomings, such as hot tearing [4,5], shrinkage porosity formation [5-9] and gas entrapment [5, 9]. As a result, these cases lead to the end products being rejected. Conversely, a new processing method that is identified as semi-solid metal (SSM) processing technique, has been employed to solve some of these conventional casting process drawbacks.

The SSM processing is known as an interesting processing method that enables the production of near net shape components of superior quality as compared to conventional casting process [10]. It allows the production of aluminium and some steel components [9]. It was first discovered by Spencer et al. [11] at the Massachusetts Institute of Technology (MIT) in the early 1970s while performing a continuous hot tearing test of solidifying Sn-15% Pb. They discovered that by shearing the molten metal during solidification process has helped to reduce its viscosity in semi-solid condition [11-13]. The SSM processing has numerous benefits, for instance superior mechanical properties, prolong die-life, reduction of solidification time and filling defects [14-17]. Moreover, it is regarded as effective in energy saving due to the lower processing temperature used than conventional casting [18]. This has led to less production cost per part [19]. The SSM processing productivity rate is found to be similar or greater as compared to the conventional high-pressure die casting process. Therefore, the implementation of this novel technology by the industry has been carried out since 1990s due to its various advantages.

Two inspection methods are normally used to check the quality of the melt, which are microstructural and elemental chemical measurements [20, 21]. However, thermal analysis is another suitable and important characterisation technique used to determine the specimen physical properties as a function of temperature (T) versus time (t) when heating or cooling the specimen based on an arranged program [22]. This method is used to assess any variations occurred within the specimen either from physical or chemical characteristics. The variations are based on the calculated properties of the thermal analysis curve. The quality of each melt is observed through documented temperatures of phase change and the

*CORRESPONDING AUTHOR | N. A. Razak | ✉ azhani@ump.edu.my

relationship between temperature and fraction solid [21]. Several thermal analysis methods are available such as differential scanning calorimetry (DSC) and differential thermal analysis (DTA). Even though DSC and DTA could give some data on melting and cooling state of any specimen, but, they failed to characterise the required parameters clearly [23]. Hence, the corresponding first derivative curves are obligatory to disclose minor peaks in regards to slight transformation heats and offer precise investigation. Therefore, an alternative, cooling curve analysis (CCA) as a non-damaging and quick method is used to check the molten metal's condition preceding to casting. Cooling curve analysis determines the relationship between alloy composition, melt treatment, cooling curve parameters and properties [21]. It is a popular method for analysis of material thermal profiles [20, 24-29] due to its low cost, simple and in particularly suitable for commercial applications [21]. Furthermore, the aforesaid methods are inadequate for examining the non-equilibrium solidification of industrial alloys [20].

Recently, a few researchers had used this method to investigate the thermal profiles of magnesium alloys [20, 23, 28] while some studied on cast aluminium alloys [24, 30]. Nevertheless, information on the thermal profiles of wrought aluminium alloy 7075 at various sample mass and solidification rates which might happen during the thixoforming process by using this method is scarce. Hence, this study aims to comprehend the correlation between solidification rate, metallurgical behaviour, and fraction solid of aluminium 7075. The resulted output from this study is significant in selecting the best processing parameters for thixoforming process.

EXPERIMENTAL PROCEDURE

Optical emission spectroscopy was used to determine the chemical composition of the wrought aluminium 7075 alloys. Six chemical composition tests were performed for obtaining precise results. Chemical composition of the wrought aluminium 7075 alloys is compared with the literature in Table 1.

Table 1. Comparison of the chemical composition of the as-received sample and the literature.

Source (wt.%)	Al	Cr	Cu	Fe	Mg	Mn	Si	Ti	Zn
As-received sample	89.8	0.27	1.33	0.22	2.26	0.05	0.16	0.07	5.74
Ahmad [31]	88.5	0.2	2.02	0.24	2.38	0.12	0.14	0.09	6.04
Bäckerud [32]	Bal	0.19	1.36	0.28	2.49	-	0.11	-	-
ASM [33]	87.1-91.4	0.18-0.28	1.2-2.0	<0.5	2.1-2.9	<0.3	<0.4	<0.2	5.1-6.1

A mass of 20-g wrought aluminium alloy 7075 was put in a graphite crucible. The graphite crucible had an inner diameter of 20 mm and a height of 40 mm. It was heated until 750 °C of temperature using an auto control high-frequency induction furnace (KX-5188 series). Then, the crucible was let to cool naturally at room temperature. This was termed as a normal cooling rate condition. Meanwhile, the intermediate and high cooling rate conditions were achieved when forced airflow with minimum and maximum speeds, respectively, was directed towards the graphite crucible. These cooling methods were based on previous work by Bäckerud et al. [32]. A calibrated Chromel-Alumel K-type thermocouple was used to determine the temperature of the melt. It is then located at the centre of the crucible and submerged to 15 mm in the melt. A data acquisition system which consists of a Data Logger GL-220 and a computer with GL software was utilised to obtain the cooling curve of temperature against time. The data logger was set at 10 Hz/ch. Cooling rates calculation were carried out between 10 to 50 °C above the liquidus temperature. The thermocouple was calibrated before the measurement of each cooling rate condition, and three repeated measurements for each condition was made. It was to ensure the results' reproducibility. The experimental setup for thermal analysis is shown in Figure 1.

Smoothing and plotting the cooling curve, along with the first derivative curve (dT/dt curve) was carried out by means of OriginPro 9 data analysis software. A baseline was then constructed on the first derivative curve. It is to symbolise the cooling rate, which could have occurred without any latent heat. It has the same trend line with the first derivative curve in the single-phase regions, which are region above the liquidus temperature, and below solidus temperature [22]. Fraction solid, f_s at specific times (Δt) was then determined by dividing the area integration value at Δt with the total area integration values measured from the start (liquidus temperature) to end (solidus temperature) of solidification as shown in Eq. (1). The concept of the area under the graph was used to calculate the area integration value, which was between the first derivative curve and baseline curve.

$$f_s = \frac{\int_{t_0}^{t_1} dH}{\int_{t_0}^{t_f} dH} = \frac{\int_{t_0}^{t_1} \left[\left. \frac{dT}{dt} \right|_{cc} - \left. \frac{dT}{dt} \right|_{bc} \right] dt}{\int_{t_0}^{t_f} \left[\left. \frac{dT}{dt} \right|_{cc} - \left. \frac{dT}{dt} \right|_{bc} \right] dt} \quad (1)$$

Samples for metallographic study were sectioned 10 mm from the bottom of the crucible, and the centre region were mounted with Bakelite thermoset phenolic resin. A hot mounting machine, Buehler Simplimet 1000 Mounting Press was used to mount the samples. The curing temperature was set at 150 °C for 1 minute and then cooled for 3 minutes. The samples were ground by using Metkon Forcipol 2V grinding machine with 320, 800, 1200, and 2400-grit size silicon carbide and flowing water for 3 minutes. The grinding wheel speed used was 250-rpm. Then, the samples were polished by using 6-, 3-, and 1-micron size diamond suspension, which was suspended on a different polishing cloth. The samples were polished for 5 minutes at each stage and polishing speed of 150 rpm. Then, the samples were finally polished with 0.05-micron size colloidal silica suspension. The etching process was carried out on the polished samples utilising Keller's reagent for almost 5 seconds. The purpose of etchant is to expose the material's grain boundaries for microscopic examination. Olympus BX51M optical microscope and Motic Images Plus 3.0 ML software was used for microstructure characterisation. The images taken were set at 10×, 20×, and 50× magnification.

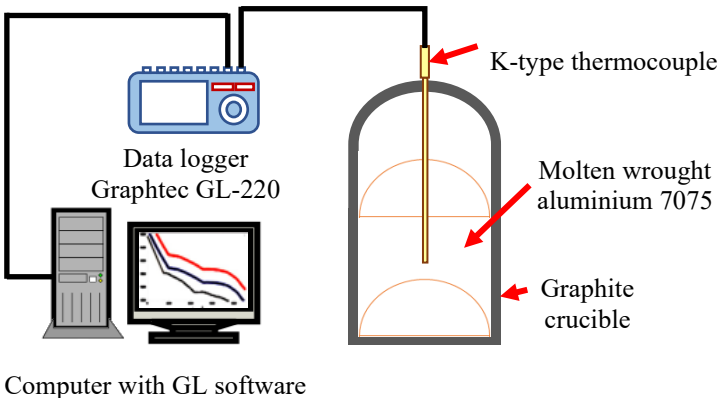

Figure 1. Schematic illustration of thermal analysis experiment setup for the normal cooling condition.

RESULTS AND DISCUSSION

Thermal Analysis

Figure 2(a) to 2(c) represents the cooling curve, its corresponding first derivative curve alongside with baseline curve, and fraction solid recorded during solidification of a normal cooling rate condition. The cooling rate was measured by the slope of the cooling curve above the liquidus region and was found to be 2.23 °C/s. Based on Figure 2(a), the liquidus, eutectic, and solidus temperature of the normal cooling rate condition were at 619.30 °C, 438.48 °C, and 421.90 °C, respectively. Meanwhile, Figure 2(b) illustrates the first derivative curve with baseline. The first derivative curve serves as an important tool to increase the accuracy of identifying phase changes during the solidification process, which might not be detected on the cooling curve. The vertical lines in Figure 2(b) represents the start and end of the solidification process of the normal cooling rate condition. Fraction solid values which were calculated between the liquidus and solidus region is shown in Figure 2(c). The information on fraction solid that happens during progressive solidification is useful to determine the processing temperature settings for semi-solid metal processing, including heating, holding and quenching temperatures.

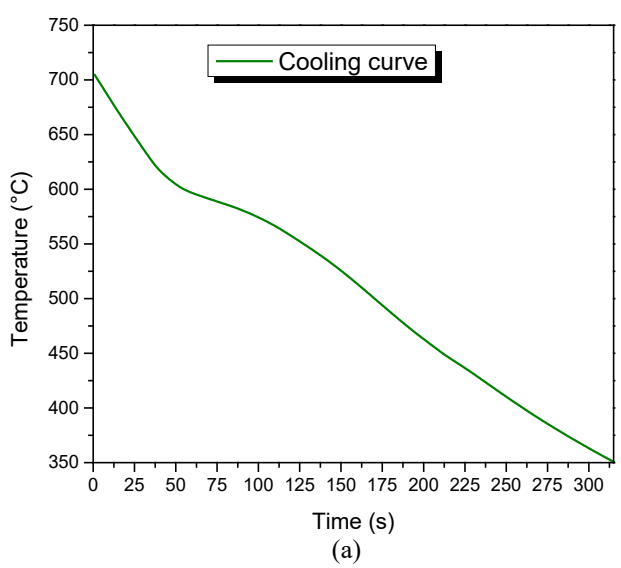

(a)

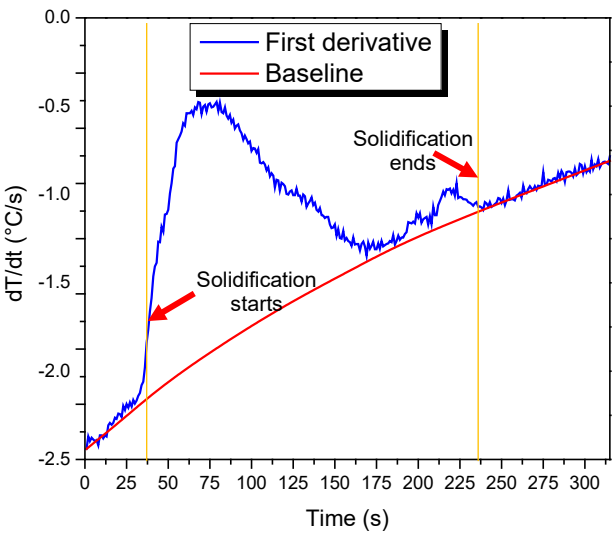

(b)

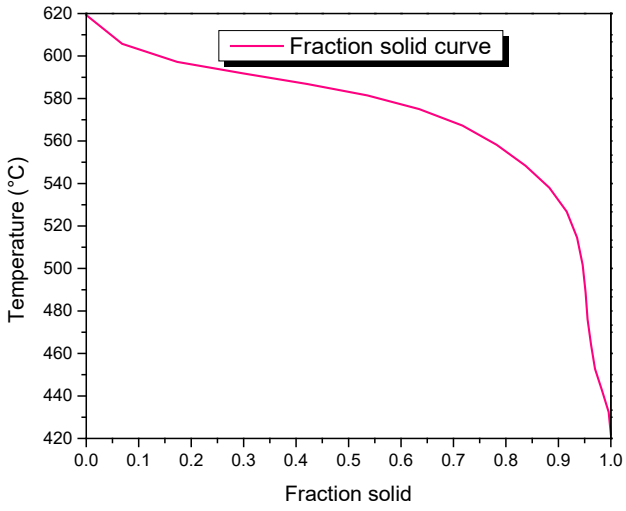

(c)

Figure 2. Thermal analysis results for a cooling rate of 2.23 °C/s, with the (a) cooling curve, (b) cooling curve derivation and a baseline against time, and (c) calculated fraction solid with respect to temperature.

Figure 3(a) shows the cooling curve for an intermediate cooling rate condition. The rate of cooling was found to be 2.88 °C/s, which was calculated at region prior to the liquidus temperature. Based on the figure, the liquidus, eutectic, and solidus temperature occurred at a temperature of 603.84 °C, 415 °C, and 393.93 °C, respectively. Meanwhile, Figure 3(b) illustrates the cooling curve first derivative, together with the baseline. The solidification start and end process of the intermediate cooling rate condition are also shown by the vertical lines in the figure. The corresponding calculated relations of temperature – fraction solid ($T_a - f_s$) is presented in Figure 3(c).

The cooling curve for high cooling rate condition is shown in Figure 4(a). The calculated cooling rate for this condition was 3.20 °C/s. The liquidus, eutectic, and solidus temperature were found at a temperature of 589.91 °C, 405.55 °C, and 385.60 °C, respectively. Figure 4(b) shows the cooling curve first derivative with a baseline, as well as vertical lines which indicate the solidification start and end process. Whereas, the corresponding calculated relations of temperature – fraction solid ($T_a - f_s$) is illustrated in Figure 4(c).

The liquidus, eutectic, and solidus temperatures of several cooling rate conditions for this experimental work, alongside data from the literature review, are shown in Table 2. Based on the results in the table, it is obvious that the results of the current research are slightly different than the findings by others. It is due to the difference in material's volume as this study takes into account only 20-g of material as compared to 60-g of material used by Bäckerud [32] and 1-kg of material used by Ahmad [31]. This has led to the difference in cooling rate, which in turn affects the phase transformation during solidification. Furthermore, the methods used in this study are different than those reported by other researchers [31-33], and this might be another reason for the difference in the results.

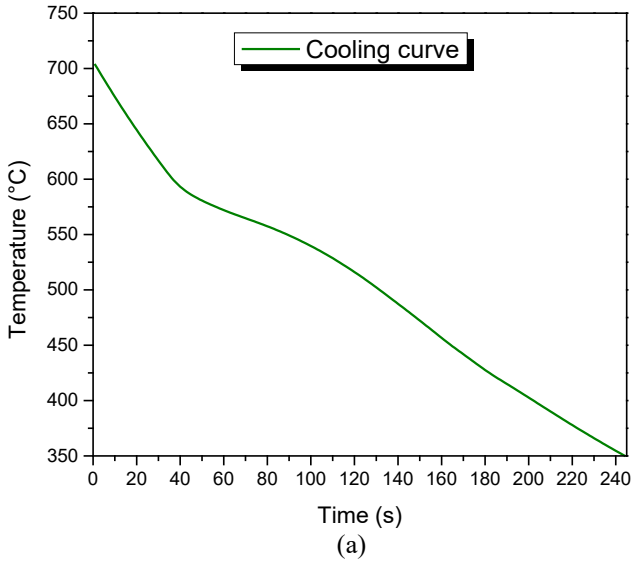

(a)

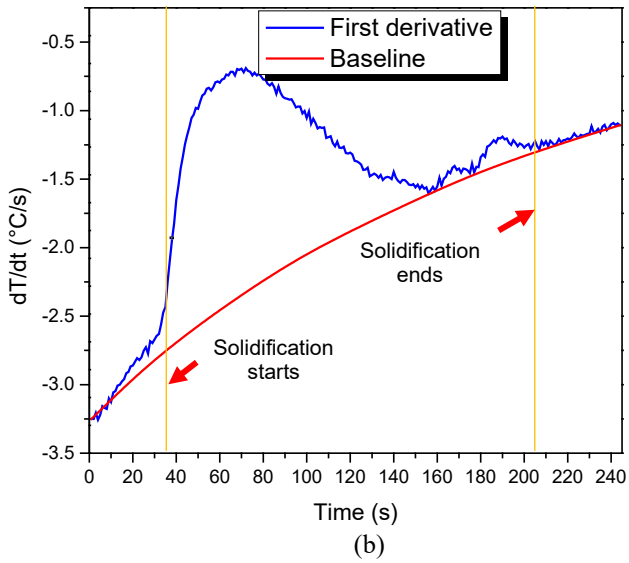

(b)

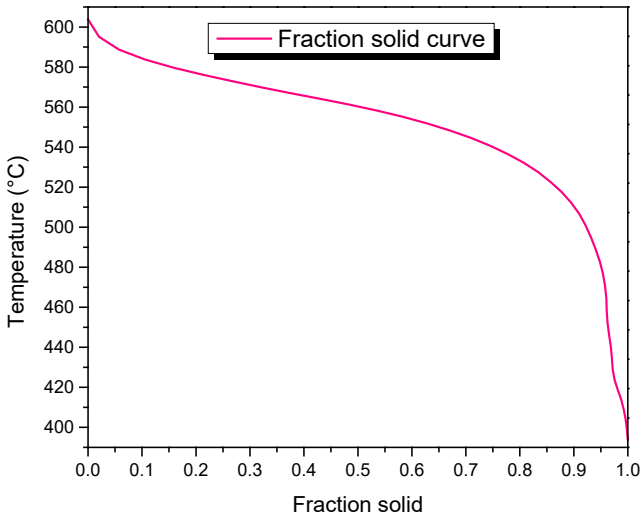

(c)

Figure 3. Thermal analysis results for a cooling rate of 2.88 °C/s, with the (a) cooling curve, (b) cooling curve derivation and a baseline against time, and (c) calculated fraction solid with respect to temperature.

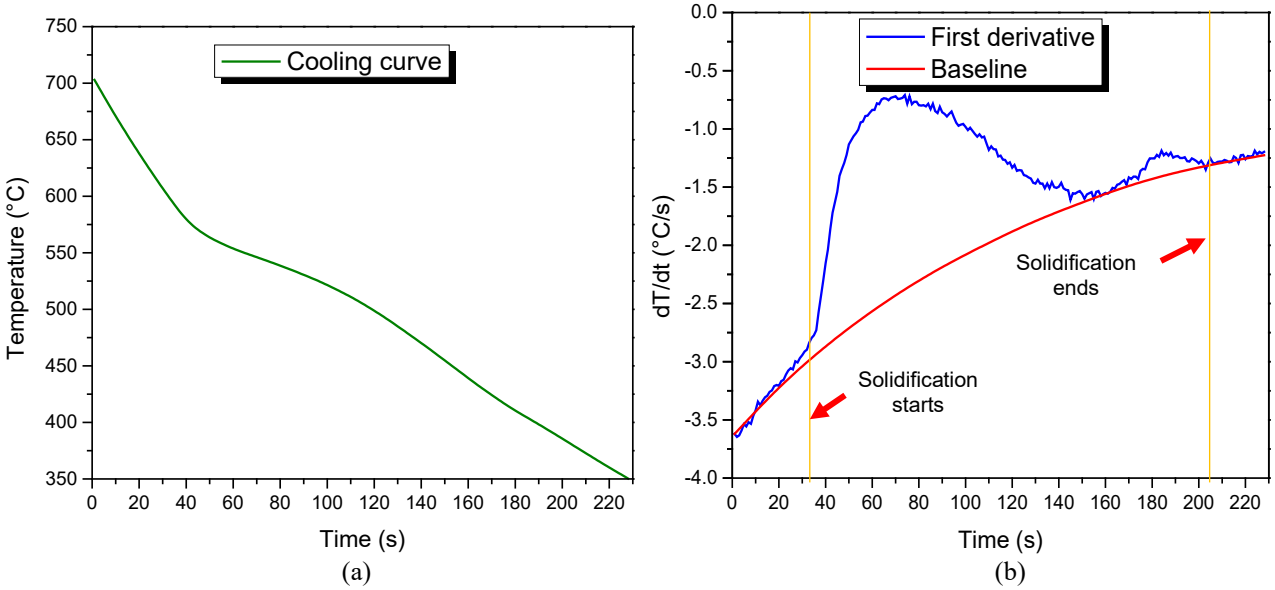

(a)

(b)

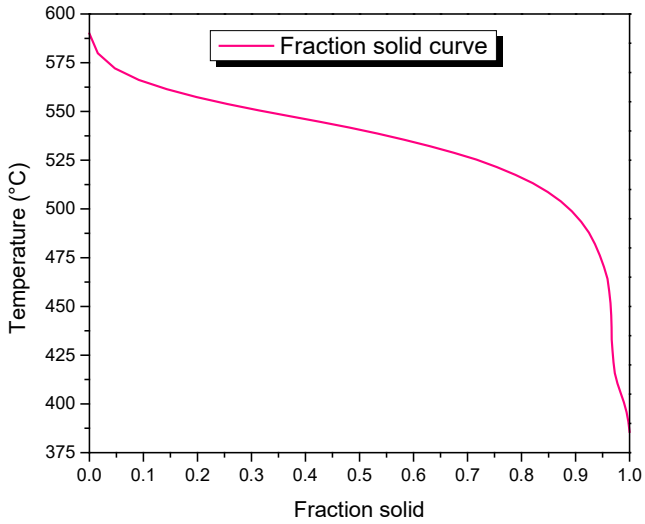

(c)

Figure 4. Thermal analysis results for a cooling rate of 3.20 °C/s, with the (a) cooling curve, (b) cooling curve derivation and a baseline against time, and (c) calculated fraction solid with respect to temperature.

Table 2. Solidification characteristic at several cooling rate conditions.

Source	Cooling rate (°C/s)	Liquidus temperature (°C)	Eutectic temperature (°C)	Solidus temperature (°C)
This work	2.23	619.30	438.48	421.90
This work	2.88	603.84	415.00	393.93
This work	3.20	589.91	405.55	385.69
Ahmad [30]	0.03	639.90	470.20	467.60
Ahmad [30]	0.21	638.00	474.70	470.20
Ahmad [30]	0.43	638.20	477.20	472.80
Bäckerud [31]	2.30	628.00	466.00	466.00
ASM [32]	-	635.00	-	477.00

Microstructure Analysis

Qualitative comparison method was chosen to analyse the impact of cooling rate on the microstructure evolution. Figure 5 shows the microstructure images of the samples' cross-sectional area for various cooling rate conditions. The area of the analysed samples was taken at the centre of the crucible after the solidification process. There was a significant contrast between the microstructure formation in the images shown. This was due to the difference in cooling rate applied. Moreover, distinct features between primary (solid) and secondary (liquid) phase can be seen in the images. The primary phase identified as α-Al was the first structure to precipitate or form throughout the solidification process. Meanwhile, the secondary phase happened to form at the primary phase grain boundary and it was the last phase to solidify.

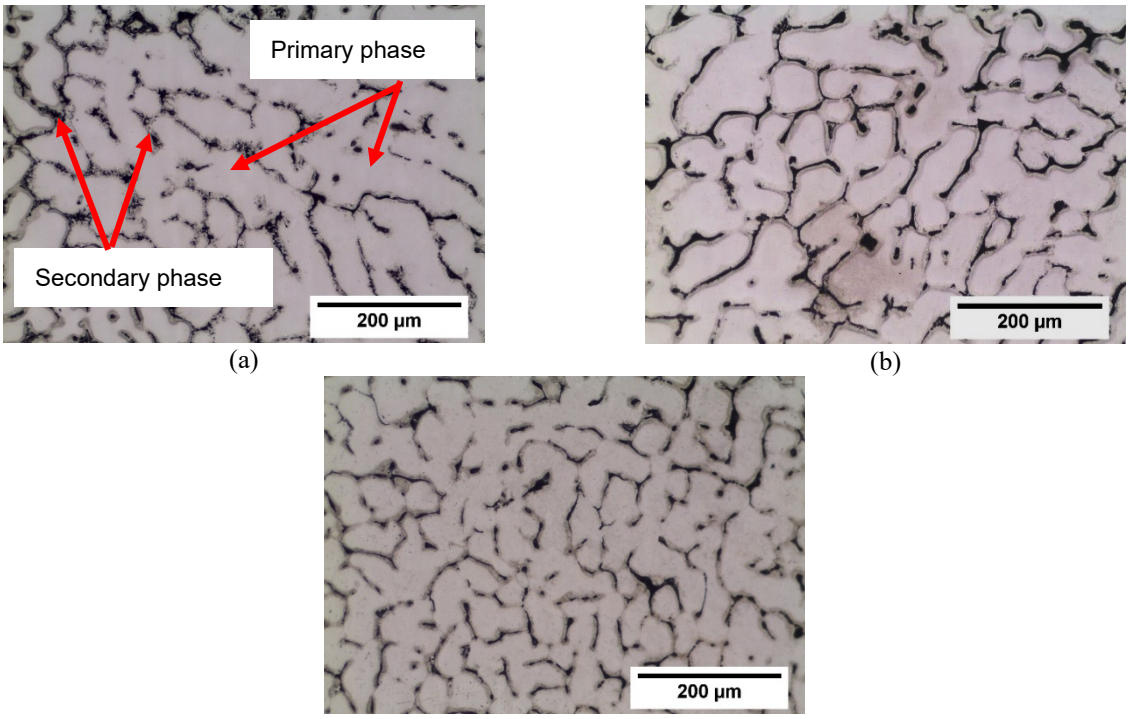

Figure 5. Microstructure evolution at the centre of solidified material with the cooling rate of (a) 2.23 °C/s, (b) 2.88 °C/s, and (c) 3.20 °C/s.

Furthermore, the quantitative method was also carried out to evaluate the formation of microstructure for each cooling rate condition. The method was used to assess the microstructure's average primary grain diameter, perimeter, circularity, and aspect ratio. Figure 6 and Figure 7 show the results of grain size measurement for microstructure at the centre of solidified material.

The formation of microstructure heavily depends on the cooling rate. The results show that the high cooling rate has led to the formation of a smaller primary grain structure. The high cooling rate of 3.20 °C/s had the smallest grain size which was measured as 96.47 µm compared to the other two cooling rate conditions. Grain size for the intermediate cooling rate was calculated to be 101.76 µm whilst the normal cooling rate had a grain size of 137.89 µm. These findings seem to be in agreement with the findings from other researchers, where the difference in cooling rate played a major contribution to microstructural changes [32, 34–36]. The increment of cooling rate enhances the extraction of heat from the melt. Thus, the melt is cooled to a temperature that is less than the equilibrium melting point. As a result, the formation of nuclei is enhanced due to the existing suitable undercooling [34]. When the cooling rates and undercooling increase, critical nuclei size reduces, which in turn modifies embryos to nuclei [24]. Furthermore, as the cooling rate increases, the

temperature range of solidification is increased, whilst, the solidification time is reduced. As the time to solidify the melt is shortened, this leads to the suppression of nuclei growth. Therefore, a higher cooling rate refines the primary grain size as illustrated in Figure 5 and 6. Other than that, the increase in cooling rate had also affected the shape of the primary grain structure. Reduction of shape factor was found when the cooling rate was increased as depicted in Figure 7. This outcome is important for developing the best parameters for SSM processing which later can be used in producing automotive parts.

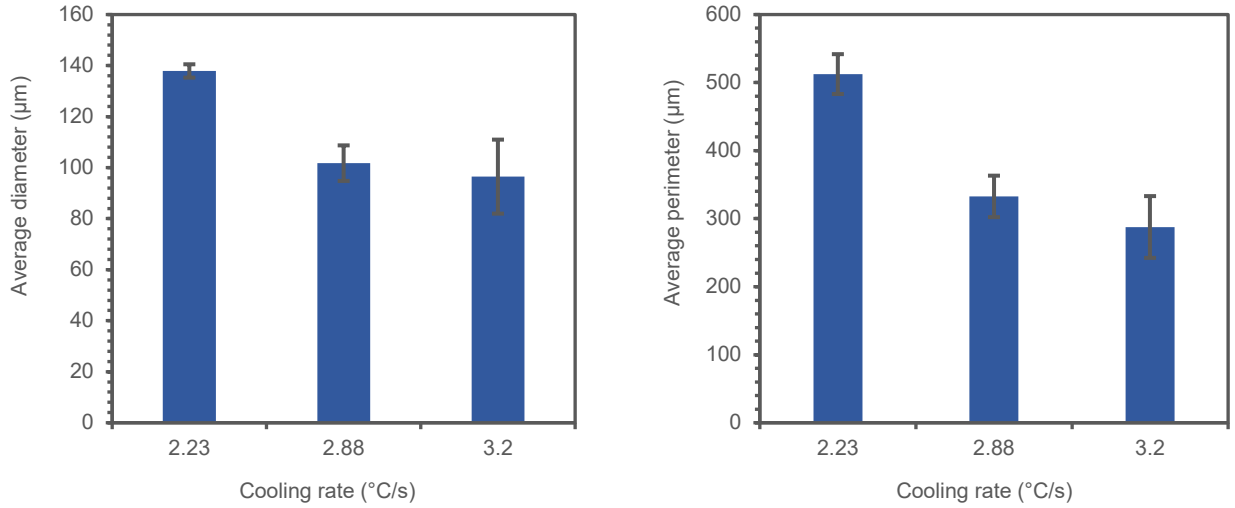

(a) (b)

Figure 6. Grain size measurement for microstructure at the centre of solidified material with (a) average primary grain diameter and (b) average primary grain perimeter where errors are 95% confidence intervals.

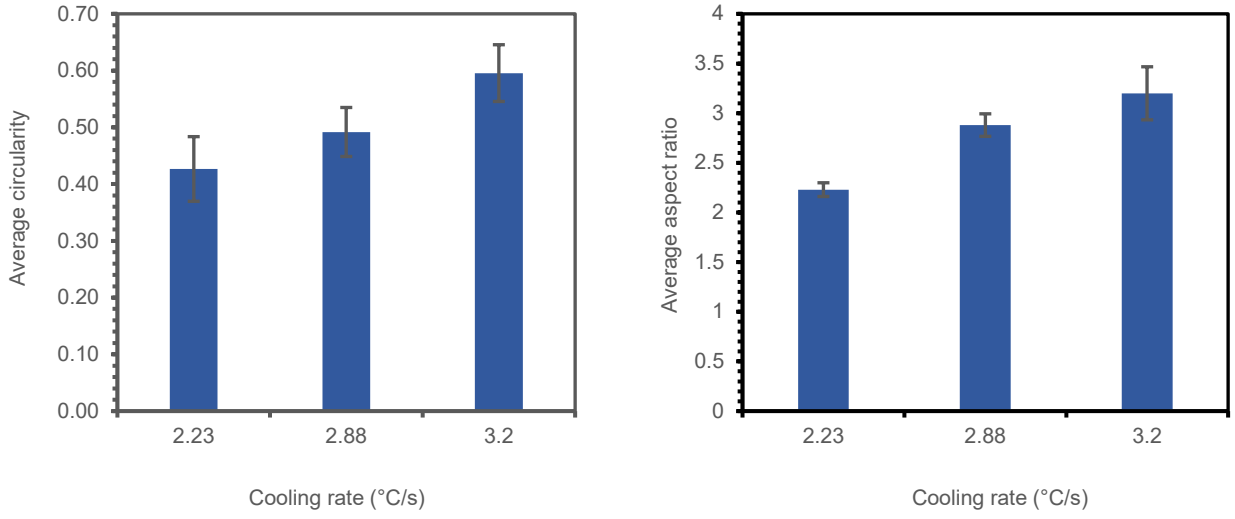

(a) (b)

Figure 7. Grain size measurement for microstructure at the centre of solidified material with (a) average primary grain circularity and (b) average primary grain aspect ratio where errors are 95% confidence intervals.

CONCLUSION

The difference in cooling rate conditions has a significant effect on the phase changes during the solidification process. The liquidus, eutectic, and solidus temperature for a normal cooling rate of 2.23 °C/s occurred at 619.30 °C, 438.48 °C, and 421.90 °C whilst for an intermediate cooling rate of 2.88 °C/s occurred at 603.84 °C, 415.0 °C, and 393.93 °C, respectively. The liquidus, eutectic, and solidus temperature for a high cooling rate of 3.20 °C/s were recorded at a lower temperature than the previous cooling rate conditions which were at 589.91 °C, 405.55 °C, and 385.69 °C. The different cooling rates also had a significant impact on the microstructure features where finer microstructure formed at the high cooling rate. The findings from this study are essential for developing the best parameters for SSM processing which later can be used in producing automotive parts.

ACKNOWLEDGEMENT

The authors would also like to acknowledge the support from Universiti Malaysia Pahang (RDU151412, RDU160311 and RDU1603125) for funding this work.

REFERENCES

[1] Polmear IJ. Light alloys, from traditional alloys to nanocrystals. Fourth. Oxford: Elsevier, 2006.

[2] Mallick PK. Overview. In: Mallick PK (ed) Materials, design and manufacturing for lightweight vehicles. Cornwall, UK: Woodhead Publishing Limited, 2010, pp. 1–32.

[3] Miller W. S, Zhuang L, Bottema J, et al. Recent development in aluminium alloys for the automotive industry. Materials Science and Engineering: A 2000; 280: 37–49.

[4] Liu F, Zhu X, Ji S. Effects of Ni on the microstructure, hot tear and mechanical properties of Al–Zn–Mg–Cu alloys under as-cast condition. Journal of Alloys and Compounds 2020; 821: 153458.

[5] Chayong S, Atkinson H V., Kapranos P. Thixoforming 7075 aluminium alloys. Materials Science and Engineering A 2005; 390: 3–12.

[6] Ma Z, Zhang H, Zhang X, et al. Rheological behaviour of partially solidified A356 alloy: Experimental study and constitutive modelling. Journal of Alloys and Compounds 2019; 803: 1141–1154.

[7] Arif MAM, Omar MZ, Sajuri Z, et al. Effects of Cu and Mg on thixoformability and mechanical properties of aluminium alloy 2014. Transactions of Nonferrous Metals Society of China (English Ed) 2020; 30: 275–287.

[8] Xiao G, Jiang J, Liu Y, et al. Recrystallization and microstructure evolution of hot extruded 7075 aluminum alloy during semi-solid isothermal treatment. Materials Characterization 2019; 156: 109874.

[9] Hu XG, Zhu Q, Midson SP, et al. Blistering in semi-solid die casting of aluminium alloys and its avoidance. Acta Materialia 2017; 124: 446–455.

[10] Pola A, Tocci M, Kapranos P. Microstructure and properties of semi-solid aluminum alloys: A literature review. Metals (Basel) 2018; 8: 1–17.

[11] Mehrabian R, Riek RG, Flemings M. Preparation and casting of metal-particulate non-metal composites. Metallurgical Transactions 1974; 5: 1899–1905.

[12] Flemings MC, Riek RG, Young KP. Rheocasting. Materials Science and Engineering, 1976; 25: 103–117.

[13] Amin-Ahmadi B, Aashuri H. Semisolid structure for M2 high speed steel prepared by cooling slope. Journal of Materials Processing Technology 2010; 210: 1632–1635.

[14] Kapranos P. Current state of semi-solid net-shape die casting. Metals (Basel); 9. Epub ahead of print 2019. DOI: 10.3390/met9121301.

[15] Luo X, Han Y, Li Q, et al. Effect of pouring temperature on microstructure and properties of A356 alloy strip by a novel semisolid micro fused-casting for metal. Journal of Wuhan University of Technology-Mater. Sci. Ed. 2019; 34: 1205–1209.

[16] Samat S, Omar MZ, Mohamed IF. Effect of feedstock geometry on the semisolid processing of Al-Si-Cu-Mg alloy. Materials Research Express 2019; 6: 2–12.

[17] Liu Z, Mao W, Wan T, et al. Study on semi-solid A380 aluminum alloy slurry prepared by water-cooling serpentine channel and its rheo-diecasting. Metals and Materials International Epub ahead of print 2020. DOI: 10.1007/s12540-020-00672-2.

[18] Lozares J, Plata G, Hurtado I, et al. Near solidus forming (NSF): Semi-solid steel forming at high solid content to obtain as-forged properties. Metals (Basel); 10. Epub ahead of print 2020. DOI: 10.3390/met10020198.

[19] Li G, Lu H, Hu X, et al. Current progress in rheoforming of wrought aluminum alloys: A review. Metals (Basel); 10. Epub ahead of print 2020. DOI: 10.3390/met10020238.

[20] Farahany S, Bakhsheshi-Rad HR, Idris MH, et al. In-situ thermal analysis and macroscopical characterization of Mg-xCa and Mg-0.5Ca-xZn alloy systems. Thermochimica Acta 2012; 527: 180–189.

[21] Emadi D, Whiting L V., Nafisi S, et al. Applications of thermal analysis in quality control of solidification processes. Journal of Thermal Analysis and Calorimetry 2005; 81: 235–242.

[22] Daniels T. Thermal analysis. London: Kogan Page Limited, 1973.

[23] Jafari H, Idris MH, Ourdjini A, et al. In situ melting and solidification assessment of AZ91D granules by computer-aided thermal analysis during investment casting process. Materials and Design 2013; 50: 181–190.

[24] Hosseini VA, Shabestari SG, Gholizadeh R. Study on the effect of cooling rate on the solidification parameters, microstructure, and mechanical properties of LM13 alloy using cooling curve thermal analysis technique. Materials and Design 2013; 50: 7–14.

[25] Ihsan-ul-haq, Shin J-S, Lee Z-H. Computer-aided cooling curve analysis of A356 aluminum alloy. Metals and Materials International 2004; 10: 89–96.

[26] Benjunior B, Ahmad AH, Rashidi MM, et al. Effect of Different Cooling Rates Condition on Thermal Profile and Microstructure of Aluminium 6061. Procedia Engineering 2017; 184: 298–305.

[27] Sedighi O, Shabestari SG, Yavari F. Investigation on the effect of Sn on solidification and microstructure of AZ91 magnesium alloy using cooling curve thermal analysis. Thermochimica Acta 2018; 667: 165–172.

[28] Naghdali S, Jafari H, Malekan M. Cooling curve thermal analysis and microstructure characterization of Mg-5Zn-1Y-xCa (0–1 wt%) alloys. Thermochimica Acta 2018; 667: 50–58.

[29] Sudheer R, Prabhu KN. A Computer Aided Cooling Curve Analysis method to study phase change materials for thermal energy storage applications. Materials and Design 2016; 95: 198–203.

[30] Chen R, Shi Y, Xu Q, et al. Effect of cooling rate on solidification parameters and microstructure of Al−7Si−0.3Mg−0.15Fe alloy. Transactions of Nonferrous Metals Society of China 2014; 24: 1645–1652.

[31] Ahmad AH, Naher S, Brabazon D. Thermal profiles and fraction solid of aluminium 7075 at different cooling rate conditions. Key Engineering Materials 2013; 554–557: 582–595.

[32] Bäckerud L, Król E, Tamminen J. Solidification characteristics of aluminium alloys; Volume 1: Wrought alloys. Oslo: Skan Aluminium, 1986.

[33] ASM International. ASM Metals Handbook, Properties and selection:nonferrous alloys and special-purpose materials. Tenth. Materials Park, OH: ASM International, 1990.

[34] Shabestari SG, Malekan M. Thermal analysis study of the effect of the cooling rate on the microstructure and solidification parameters of 319 aluminum alloy. Canadian Metallurgical Quarterly 2005; 44: 305–312.

[35] Ahmad AH, Naher S, Brabazon D. Effects of cooling rates on thermal profiles and microstructure of aluminium 7075. International Journal of Automotive and Mechanical Engineering 2014; 9: 1685–1694.

[36] Bünck M, Warnken N, Bührig-Polaczek A. Microstructure evolution of rheo-cast A356 aluminium alloy in consideration of different cooling conditions by means of the cooling channel process. Journal of Materials Processing Technology 2010; 210: 624–630.